

# Crystal Field and Dzyaloshinsky-Moriya Interaction in orbitally ordered $\text{La}_{0.95}\text{Sr}_{0.05}\text{MnO}_3$ : An ESR Study

J. Deisenhofer <sup>a</sup>, M. V. Eremin <sup>a,b</sup>, D. V. Zakharov <sup>b</sup>, V. A. Ivanshin <sup>a,b</sup>, R. M. Eremina <sup>a,c</sup>, H.-A. Krug von Nidda <sup>a</sup>, A. A. Mukhin <sup>d</sup>, A. M. Balbashov <sup>e</sup>, and A. Loidl <sup>a</sup>

<sup>a</sup> *Experimentalphysik V, EKM, Universität Augsburg, 86135 Augsburg, Germany*

<sup>b</sup> *Kazan State University, 420008 Kazan, Russia*

<sup>c</sup> *E. K. Zavoisky Physical-Technical Institute, 420029 Kazan, Russia*

<sup>d</sup> *Institut of General Physics, Russian Academy of Sciences, 117942 Moscow, Russia*

<sup>e</sup> *Moscow Power Engineering Institute, 105835 Moscow, Russia*

(Dated: November 9, 2018)

We present a comprehensive analysis of Dzyaloshinsky-Moriya interaction and crystal-field parameters using the angular dependence of the paramagnetic resonance shift and linewidth in single crystals of  $\text{La}_{0.95}\text{Sr}_{0.05}\text{MnO}_3$  within the orthorhombic Jahn-Teller distorted phase. The Dzyaloshinsky-Moriya interaction ( $\sim 1$  K) results from the tilting of the  $\text{MnO}_6$  octahedra against each other. The crystal-field parameters  $D$  and  $E$  are found to be of comparable magnitude ( $\sim 1$  K) with  $D \approx -E$ . This indicates a strong mixing of the  $|3z^2 - r^2\rangle$  and  $|x^2 - y^2\rangle$  states for the real orbital configuration.

PACS numbers: 76.30.-v, 71.70.Ej, 75.30.Et, 75.30.Vn

## INTRODUCTION

The importance of orbital degrees of freedom in understanding the complex phase diagrams of the manganites [1] is subject of intense research activities (see e.g. references [2, 3, 4] for an overview). The antiferromagnetic insulator  $\text{LaMnO}_3$  ( $T_N = 140$  K) is an orbitally ordered system [5], which has been established experimentally by resonant X-ray scattering [6] and neutron diffraction [7]. Moreover, Saitoh *et al.* recently reported evidence for orbital excitations by Raman spectroscopy [8]. The orbital order in  $\text{LaMnO}_3$  is induced by the cooperative Jahn-Teller (JT) effect of the  $\text{Mn}^{3+}$  ions (electronic configuration  $3d^4$  :  $t_{2g}^3 e_g^1$ , spin  $S = 2$ ), which at temperatures  $T < T_{\text{JT}} = 750$  K leads to a strong orthorhombic distortion of the perovskite structure. In the paramagnetic state electron spin resonance (ESR) reveals a single exchange-narrowed resonance line with a  $g$  value near 2.0 due to all  $\text{Mn}^{3+}$  ions [9] and hence directly probes the spin of interest. Doping divalent ions like Sr or Ca onto the  $\text{La}^{3+}$  place gradually suppresses the JT distortion and leads to a ferromagnetic insulating and finally to a metallic phase at approximately 15% Sr doping.

In a previous work, we presented a systematic ESR study in single crystals of  $\text{La}_{1-x}\text{Sr}_x\text{MnO}_3$  with Sr concentrations  $0 \leq x \leq 0.2$  [10]. In the JT distorted phase the resonance linewidth  $\Delta H$  is strongly enhanced compared to the undistorted phase, reaching maximum values of about  $\Delta H_{\text{max}} \approx 2.5$  kOe. Similar results were reported from polycrystalline  $\text{La}_{1-x}\text{Ca}_x\text{MnO}_3$  [11] and oxygen doped ceramic  $\text{LaMnO}_{3+\delta}$  [12]. Moreover, the single crystals exhibit a pronounced anisotropy of the resonance linewidth in the Jahn-Teller distorted phase, which disappears at temperatures  $T > T_{\text{JT}}$ . The pure  $\text{LaMnO}_3$  sample turned out to be strongly twinned and therefore did not allow a detailed analysis of the angular

dependence. Instead, the  $\text{La}_{0.95}\text{Sr}_{0.05}\text{MnO}_3$  crystal was found to be untwinned and can effectively be treated like the mother compound ( $x = 0$ ), as it is still an antiferromagnetic insulator ( $T_N = 140$  K) showing a similar magnetic susceptibility. Only the JT transition is shifted to lower temperatures, with  $T_{\text{JT}}(x = 0.05) = 600$  K.

In a first approach [10], we ascribed the orientation dependence of the ESR linewidth to the influence of the Dzyaloshinsky-Moriya (DM) interaction, which arises from the tilting of the  $\text{MnO}_6$  octahedra along the antiferromagnetically coupled  $b$  axis, only. However, the orthorhombic distortion of the  $\text{MnO}_6$  octahedra itself gives rise to a crystal-field (CF) induced line broadening of comparable order of magnitude [11] and for a complete description one has also to take into account the DM interaction via Mn-O-Mn bonds within the ferromagnetically coupled  $ac$  plane, which is smaller than along the  $b$  axis but not negligible.

In the present paper, we study the angular dependence of the resonance linewidth in the paramagnetic regime at temperatures  $T > T_N$ . The contributions of CF and DM interaction consist of the superposition of the four non equivalent Mn ions in the orthorhombic unit cell. The evaluation is based on the structural data for  $\text{LaMnO}_3$  determined from neutron scattering experiments by Huang *et al.* [13]. The application to the experimental angular dependence of the ESR linewidth at 200K and 300K allows to estimate the microscopic CF parameters  $D$  and  $E$  and the DM vectors for all Mn-Mn pairs. Throughout this paper we will use the crystallographic notation following Huang *et al.*, where the  $b$  axis (instead of the former  $c$  axis in reference [10]) denotes the direction perpendicular to the ferromagnetically coupled  $ac$  planes.

## EXPERIMENT

The ESR measurements were performed with a Bruker ELEXSYS E500 CW-spectrometer at X-band frequency ( $\nu \approx 9.35$  GHz), equipped with continuous gas-flow cryostats for He (Oxford Instruments) and N<sub>2</sub> (Bruker), which allow to cover a temperature range between 4.2 K and 680 K. The ESR spectra record the power  $P$  absorbed by the sample from the transverse magnetic microwave field as a function of the static magnetic field  $H$ . The signal-to-noise ratio of the spectra is improved by detecting the derivative  $dP/dH$  with lock-in technique. A small single crystal of La<sub>0.95</sub>Sr<sub>0.05</sub>MnO<sub>3</sub> (volume 2 mm<sup>3</sup>) was fixed on a suprasil quartz rod with low-temperature glue (General Electrics), which allowed the rotation of the sample around defined crystallographic axes. We

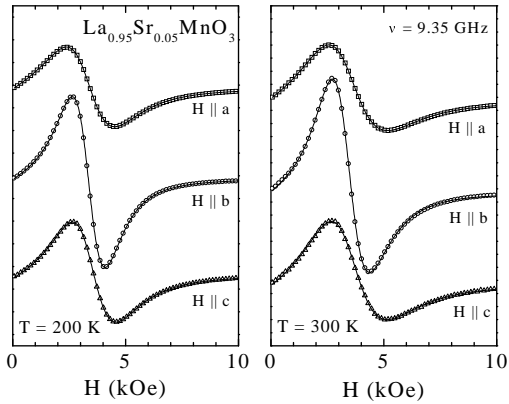


FIG. 1: ESR spectra of La<sub>0.95</sub>Sr<sub>0.05</sub>MnO<sub>3</sub> at 200 K (left hand side) and 300 K (right hand side) for the magnetic field  $H$  applied parallel to the crystallographic axis ( $a, b, c$ ). Solid lines represent the fits using the Dysonian line shape, equation 1.

measured the angular dependence of the paramagnetic resonance with respect to the orientation of the static magnetic field  $H$  in the three crystallographic planes ( $ab$ ,  $ac$ , and  $bc$ ) at temperatures 200 K and 300 K, deeply in the Jahn-Teller distorted orthorhombic phase. Figure 1 illustrates typical ESR spectra for the magnetic field applied parallel to the three main axes. In all cases, one observes a broad, exchange-narrowed resonance line, which is well fitted by a Dysonian line shape [14] given by

$$\frac{dP}{dH} \propto \frac{d}{dH} \left\{ \frac{\Delta H + \alpha(H - H_{\text{res}})}{(H - H_{\text{res}})^2 + \Delta H^2} + \frac{\Delta H + \alpha(H + H_{\text{res}})}{(H + H_{\text{res}})^2 + \Delta H^2} \right\} \quad (1)$$

This is an asymmetric Lorentzian line, which includes both absorption and dispersion, where  $\alpha$  denotes the dispersion-to-absorption (D/A) ratio. As the linewidth  $\Delta H$  is of the same order of magnitude as the resonance

field  $H_{\text{res}}$  in the present compounds, eq. (1) takes into account both circular components of the exciting linearly polarized microwave field and therefore also includes the resonance at reversed magnetic field  $-H_{\text{res}}$ .

Such asymmetric line shapes are usually observed in metals, where the skin effect drives electric and magnetic microwave components in the sample out of phase and therefore leads to an admixture of dispersion into the absorption spectra. For samples small compared to the skin depth one expects a symmetric absorption spectrum ( $\alpha = 0$ ), whereas for samples large compared to the skin depth absorption and dispersion are of equal strength yielding an asymmetric resonance line ( $\alpha = 1$ ). A second reason for the asymmetry, which also occurs in insulators, arises from the influence of non diagonal elements of the dynamic susceptibility: In systems with interactions of low symmetry and sufficiently broad resonance lines ( $H_{\text{res}} \approx \Delta H$ ) the line shape shows characteristic distortions depending on the frequency and orientation of the exciting microwave field [15], where eq. (1) yields a useful approximation of the spectrum.

Comparing the spectra at 200 K with those at 300 K one recognizes an increasing asymmetry with increasing temperature: The average D/A ratio increases from about 0.05 at 200 K to 0.35 at 300 K. This can be understood in terms of the skin effect due to the increase of the conductivity with increasing temperature. The resistivity  $\rho$  of the sample under investigation is about 500  $\Omega$ cm at 200 K and 10  $\Omega$ cm at 300 K [16]. We estimated [10] that for resistivities  $\rho < 1 \Omega$ cm the skin depth becomes smaller than the dimensions of the sample, which are about 1 mm. As the skin depth is proportional to the square root of the resistivity, the influence of the skin effect becomes visible even at 300 K. However at 200 K, it can be neglected. The remaining asymmetry, which will be discussed in connection with the resonance field below, has to be ascribed to the non diagonal contributions of the dynamic susceptibility.

Figures 2 and 3 show the full angular dependence of linewidth (upper frame), resonance field (lower frame) and D/A ratio (middle frame) for 200 K and 300 K, as obtained from the fit with eq. 1. The linewidth exhibits a pronounced anisotropy with respect to the crystallographic  $b$  axis and a weaker angular dependence within the  $ac$  plane, which can be empirically described by a  $\cos^2$ -law. The D/A ratio depends on the orientation of the microwave field, which is applied parallel to the rotation axis, and even becomes negative at 200 K, if the microwave field is perpendicular to the  $ac$  plane. This cannot be understood in terms of the skin effect alone, which always produces a positive D/A ratio. Moreover, the influence of the skin effect should be negligible at 200 K. Hence, the asymmetry has to be ascribed partly to the influence of the non diagonal elements of the dynamic susceptibility. The angular dependence of the resonance field exhibits additional 90° modulations. They

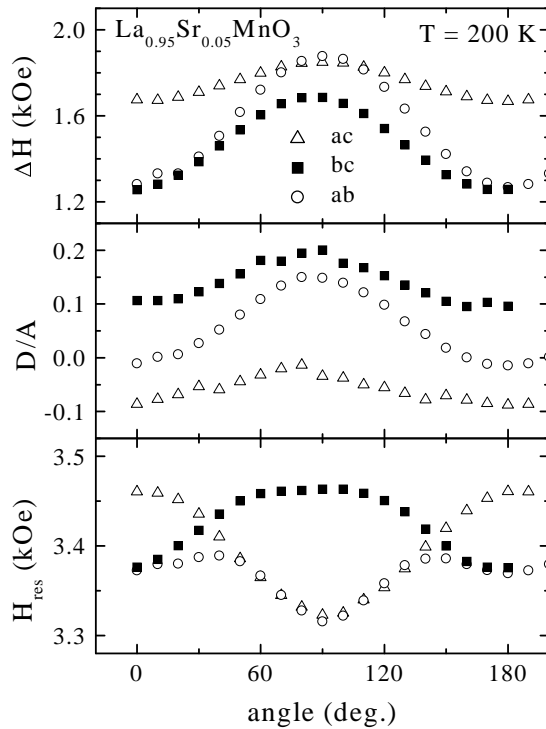


FIG. 2: Angular dependence of linewidth  $\Delta H$  (upper frame), D/A ratio (middle frame), and resonance field  $H_{\text{res}}$  (lower frame) in  $\text{La}_{0.95}\text{Sr}_{0.05}\text{MnO}_3$  for the magnetic field applied within the three crystallographic planes at 200 K

appear to be strongest for the *ab* plane, where the D/A ratio exhibits the most pronounced angular dependence. At the same time the D/A ratio is strongly correlated with the resonance linewidth, as they both attain their maximum values at the same angle. However, for these broad signals, the baseline is not so well defined as in the case of narrow lines and a shift in the D/A ratio can be compensated by resonance field and baseline. For this reason, the angular dependence of the D/A ratio can be an artificial effect, which is probably related to the large linewidth. Hence, we tried to fit the ESR spectra with a constant average D/A ratio for each rotation plane. It turned out that the spectra at 200 K can be satisfactorily fitted as well. This procedure has no visible influence on the linewidth, but the resonance field is clearly changed, as can be obtained from Fig. 6, which shows the corrected data for 200 K. The amplitude of the anisotropy remains approximately unchanged, but the additional 90° modulations more or less disappear. Turning to the resonance field data at 300 K, the situation is more complicated, as the influence of the skin effect becomes important, too. The amplitude of the D/A-angular dependence increases

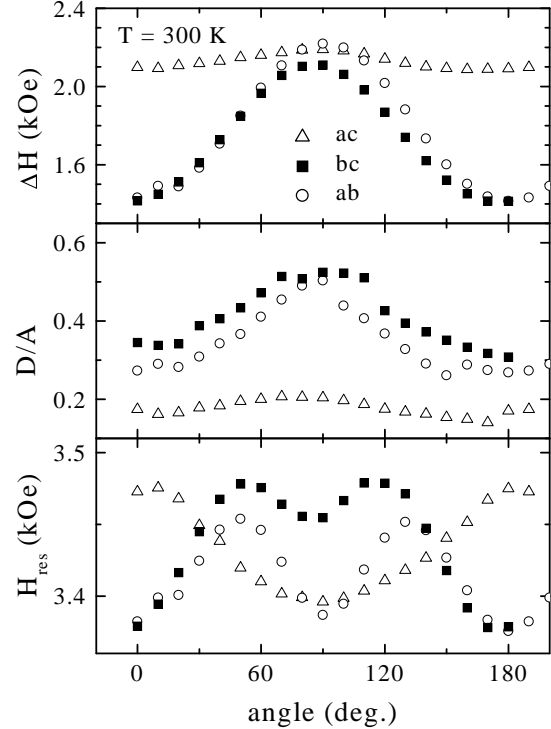


FIG. 3: Angular dependence of linewidth  $\Delta H$  (upper frame), D/A ratio (middle frame), and resonance field  $H_{\text{res}}$  (lower frame) in  $\text{La}_{0.95}\text{Sr}_{0.05}\text{MnO}_3$  for the magnetic field applied within the three crystallographic planes at 300 K

and a fit with a constant D/A ratio is not satisfactory anymore. Therefore we omit a correction of the resonance fields at 300 K.

## THEORETICAL BACKGROUND

A strongly exchange coupled magnetic system like  $\text{LaMnO}_3$  can be described by the following Hamiltonian

$$\mathcal{H} = J \sum_{(i < j)} \mathbf{S}_i \cdot \mathbf{S}_j - \mu_B \sum_i \mathbf{H} \cdot \mathbf{g} \cdot \mathbf{S}_i + \mathcal{H}_{\text{int}} \quad (2)$$

where the first term describes the superexchange interaction between two next-neighbor Mn spins  $\mathbf{S}_i$  and  $\mathbf{S}_j$  with coupling constant  $J$ . The second term describes the Zeeman splitting of the spin states with gyromagnetic tensor  $\mathbf{g}$  within an external magnetic field  $\mathbf{H}$ , where  $\mu_B$  denotes the Bohr magneton. The third term  $\mathcal{H}_{\text{int}}$  includes all interactions, which do not conserve the total spin and therefore contribute to the broadening of the ESR line as there are CF, DM interaction, anisotropic

exchange (AE) interaction, dipole-dipole interaction, and hyper-fine interaction. Due to estimation of their relative strength [11] it turned out that CF and DM interaction yield by far the largest contribution.

## Interactions

To derive the appropriate expressions for CF and DM interaction, we use the structural parameters of the  $\text{LaMnO}_3$ -IIa sample (space group  $Pnma$ ) determined by Huang *et al.* [13], because it shows an antiferromagnetic ground state and an ordering temperature of about 140 K, which is consistent with the magnetic properties of our sample [17]. Figure 7(a) in reference [13] shows the crystallographic structure of  $\text{LaMnO}_3$  in the strongly Jahn-Teller distorted phase. Due to the tilting of the  $\text{MnO}_6$  octahedra one can identify four inequivalent positions of manganese ions in the orthorhombic unit cell, which is illustrated in Fig. 7(b) of the same reference [13].

### Crystal Field

In a local coordinate system, where the axes are directed along the Mn-O bonds of the  $\text{MnO}_6$  octahedra, the spin Hamiltonian is usually written in cartesian spin components ( $S_x, S_y, S_z$ ) with parameters  $D$  and  $E$  as [18]

$$\mathcal{H}^{\text{CF}} = DS_z^2 + E(S_x^2 - S_y^2) \quad (3)$$

where the  $z$  axis is directed along the longest Mn-O link close to the  $ac$  plane and the  $y$  axis is parallel to Mn-O(1) bond almost along the  $b$  direction. Small orthorhombic distortions of the  $\text{MnO}_6$  octahedron will be neglected in this section. Because the linewidth is invariant under shift transformations, we can redefine  $\mathcal{H}^{\text{CF}}$  for simplification as

$$\begin{aligned} \mathcal{H}^{\text{CF}} &= DS_z^2 + E(S_x^2 - S_y^2) - E(S_z^2 + S_x^2 + S_y^2) \\ &= D'S_z^2 + E'S_y^2 \end{aligned} \quad (4)$$

where  $D' = D - E$  and  $E' = -2E$ . It is useful to recall that the  $y$  axis is almost parallel to  $b$ . The octahedra are rotated with respect to their next neighbor within the unit cell. Therefore in the crystallographic system  $(a, b, c)$  we have different crystal-field components at the four inequivalent Mn places which are listed in table I.

The CF components for the Mn ion at  $(0, 0, \frac{1}{2})$  read

$$\begin{aligned} D_{xx}^{(1)} &= (\frac{1}{2} - x)^2 (\frac{a}{R_l})^2 D' + (\frac{1}{2} - X)^2 (\frac{a}{R_m})^2 E' \quad (5) \\ D_{yy}^{(1)} &= (\frac{yb}{R_l})^2 D' + (\frac{b}{4R_m})^2 E' \\ D_{zz}^{(1)} &= (\frac{zc}{R_l})^2 D' + (\frac{Zc}{R_m})^2 E' \\ D_{xy}^{(1)} &= (x - \frac{1}{2}) \frac{ayb}{R_l^2} D' + (X - \frac{1}{2}) \frac{ab}{4R_m^2} E' \\ D_{xz}^{(1)} &= (\frac{1}{2} - x) \frac{azc}{R_l^2} D' + (\frac{1}{2} - X) \frac{aZc}{R_m^2} E' \\ D_{yz}^{(1)} &= -\frac{ybzc}{R_l^2} D' - \frac{bZc}{4R_m^2} E' \end{aligned}$$

Long, middle and short Mn-O distances in square are

$$\begin{aligned} R_l^2 &= (x - \frac{1}{2})^2 a^2 + (yb)^2 + (zc)^2 \quad (6) \\ R_m^2 &= (X - \frac{1}{2})^2 a^2 + (\frac{b}{4})^2 + (Zc)^2 \\ R_s^2 &= (xa)^2 + (yb)^2 + (\frac{1}{2} + z)^2 c^2 \end{aligned}$$

Here capital  $X, Z$  and small letters  $x, y, z$  denote the structure parameters (after Huang *et al.* [13]) for the oxygen ions along  $b$  and within the  $ac$  plane respectively.

### Dzyaloshinsky-Moriya Interaction

The Hamiltonian, which describes the antisymmetric DM interaction [19], can be written as

$$\mathcal{H}_{DM} = \mathbf{G}_{ij} \cdot [\mathbf{S}_i \times \mathbf{S}_j], \quad (7)$$

with the DM vector  $\mathbf{G}_{ij} = d_{ij} \cdot [\mathbf{n}_{Oi} \times \mathbf{n}_{Oj}]$  being perpendicular to the plane defined by a Mn ion at site  $(i)$ , the bridge ligand O, and a Mn ion at site  $(j)$ , where  $\mathbf{n}$  are unit vectors along  $\text{Mn}^{3+}$ - $\text{O}^{2-}$  bonds [20, 21]. The intrinsic scalar parameter  $d_{ij}$  strongly depends on the orbital states and the Mn-O-Mn bridge angle. In the case of pure  $\text{LaMnO}_3$  both the tilting and the JT distortion of the  $\text{MnO}_6$  octahedra account for the origin of antisymmetric contributions to the superexchange interaction between the Mn ions. A necessary condition for the existence of DM contributions is the lack of a center of inversion between the magnetic ions [19]. With the apical oxygen being shifted away from the  $[010]$  axis, there is a rather strong DM coupling between the  $ac$  planes and a smaller coupling within the  $ac$  planes. Figure 4 depicts all next-neighbor couplings that give rise to a DM interaction. For the  $Pnma$  structure, the components  $G_{ij}^\alpha$  ( $\alpha = x, y, z$ ) of the DM vectors of all Mn pairs within the unit cell are listed in table II. The index  $j = 1 \dots 4$

## Resonance Field

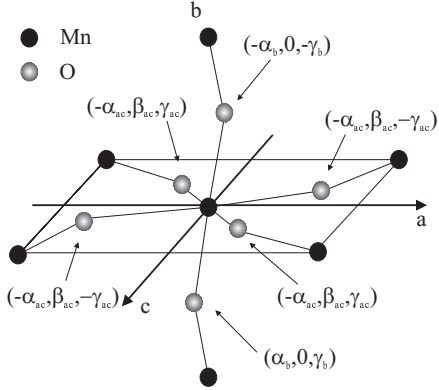


FIG. 4: Next-neighbor bonds of the Mn ions.  $\alpha$ ,  $\beta$ , and  $\gamma$  denote the cartesian components of the DM vector  $\mathbf{G}_{ij}$ .

denotes the four magnetically inequivalent positions of the Mn ion in the unit cell. The index  $i = 1\dots 6$  refers to the six next neighbors around each Mn site with number  $j$ , as it is shown in Fig. 4. The absolute values can be expressed via two parameters  $d_1$  (inter  $ac$  plane) and  $d_2$  (intra  $ac$  plane) as

$$\begin{aligned}
\alpha_b &= d_1 \frac{Z}{2} \frac{bc}{R_m^2} \\
\beta_b &= 0 \\
\gamma_b &= d_1 \frac{1}{2} \left( X - \frac{1}{2} \right) \frac{ab}{R_m^2} \\
\alpha_{ac} &= d_2 \frac{y}{2} \frac{bc}{R_l R_s} \\
\beta_{ac} &= d_2 \frac{1}{2} \left( x - z - \frac{1}{2} \right) \frac{ac}{R_l R_s} \\
\gamma_{ac} &= d_2 \frac{y}{2} \frac{ab}{R_l R_s}
\end{aligned} \tag{8}$$

where  $R_m$  measures the Mn-O distance along the antiferromagnetically coupled  $b$  direction and  $R_l$  and  $R_s$  denote the Mn-O distances within the ferromagnetically coupled  $ac$ -plane. A microscopic expression for  $d_1$  and  $d_2$  is discussed in Appendix 1.

The resonance field of the strongly exchange narrowed ESR line is generally determined by the first moment of the spectrum. Here we choose another approach, which also allows to take into account the demagnetization effect. Hence, we start from the equation of motion [22]:

$$\begin{aligned} \frac{\partial S^+}{\partial t} &= ig\mu_B \left\{ H - \frac{M}{2} (2N_{zz} - N_{xx} - N_{yy}) \right\} S^+ \\ &+ \frac{1}{i\hbar} [S^+, H_{\text{int}}] + ig\mu_B M (N_{xx} - N_{yy}) S^- \quad (9) \end{aligned}$$

with the magnetization  $M$  and the demagnetizing factors  $N_{\alpha\alpha}$ . The circular spin operators are defined as usual  $S^{\pm} = S_x \pm iS_y$ . Here we assume an isotropic  $g$  value, because the influence of the AE interaction can be neglected with respect to the crystal field. The DM interaction does not contribute to the resonance shift, because the expectation value of the commutator  $\langle [S^+, H^{\text{DM}}] \rangle$  vanishes. After linearization the expectation value of the commutator  $\langle [S^+, H_{\text{int}}] \rangle$  is given by

$$\begin{aligned} \langle [S^+, H^{\text{CF}}] \rangle &\approx \frac{M_{\text{at}}}{g\mu_B} \frac{1}{4} \sum_j (\tilde{D}_{xx}^{(j)} - \tilde{D}_{yy}^{(j)} + 2i\tilde{D}_{xy}^{(j)}) S^- \\ &+ \frac{M_{\text{at}}}{g\mu_B} \frac{1}{4} \sum_j (\tilde{D}_{xx}^{(j)} + \tilde{D}_{yy}^{(j)} - 2\tilde{D}_{zz}^{(j)}) S^+ \end{aligned} \quad (10)$$

Here  $M_{\text{at}} = (g\mu_B)^2 S(S+1)H/[3k(T - \Theta_{\text{CW}})]$  is the magnetization per one Mn site, and  $\Theta_{\text{CW}} = 111$  K is the paramagnetic Curie-Weiss temperature. The crystal-field components  $\tilde{D}_{\alpha\beta}$  refer to the coordinate system, in which the external field determines the  $z$  axis and are related to the components  $D_{\alpha\beta}$  in the crystallographic system via the usual transformation rules (see Appendix 2). The sum  $(j)$  is running over the four inequivalent Mn positions of the unit cell. If we further neglect the demagnetization effect, which according to [22] is relatively small in the paramagnetic regime, the ESR frequency reads

$$\begin{aligned}
(h\nu)^2 &= [g\mu_B H + \frac{M_{\text{at}}}{4g\mu_B} \sum_j (\tilde{D}_{xx}^{(j)} + \tilde{D}_{yy}^{(j)} - 2\tilde{D}_{zz}^{(j)})] \quad (11) \\
&- \frac{M_{\text{at}}}{4g\mu_B} \sum_j [(\tilde{D}_{xx}^{(j)} - \tilde{D}_{yy}^{(j)} + 2i\tilde{D}_{xy}^{(j)})] \\
&\times [(\tilde{D}_{xx}^{(j)} - \tilde{D}_{yy}^{(j)} - 2i\tilde{D}_{xy}^{(j)})]
\end{aligned}$$

The angular dependence of the resonance field  $H_{\text{res}}(\theta, \varphi)$  is obtained after substitution of  $\tilde{D}_{\alpha\beta}$  by  $D_{\alpha\beta}$  (see Appendix 2). Polar angle  $\theta$  and azimuth angle  $\varphi$  are measured with respect to the  $c$  and  $a$  axes of the orthorhombic unit cell.

## Linewidth

In the case of strong exchange narrowing ( $\mathcal{H}_{\text{ex}} \gg \mathcal{H}_{\text{int}}$ ), the ESR linewidth  $\Delta H$  is determined by the second moment  $M_2$  of the resonance line divided by the exchange frequency  $\omega_{\text{ex}}$  [23]

$$\Delta H \simeq \frac{1}{g\mu_{\text{B}}\hbar} \frac{M_2}{\omega_{\text{ex}}} \quad (12)$$

In the present case the second moment is determined by the sum of DM and CF contributions ( $M_2^{\text{DM}} + M_2^{\text{CF}}$ )

Within the coordinate system, where the  $z$  axis is determined by the external magnetic field, the second moment due to Dzyaloshinsky-Moriya interaction is calculated as [24, 25]

$$M_2^{\text{DM}} = \frac{2}{3}S(S+1) \sum_{i,j} \left[ (\tilde{G}_{ij}^x)^2 + (\tilde{G}_{ij}^y)^2 + 2(\tilde{G}_{ij}^z)^2 \right] \quad (13)$$

The index  $j = 1 \dots 4$  is running over all four magnetically inequivalent positions of the Mn ion in the unit cell. The sum over index  $i = 1 \dots 6$  refers to the six next Mn neighbors around each Mn site with number  $j$ . After transformation into the crystallographic system and using the values listed in table II, the average over all four positions yields the angular dependence

$$\begin{aligned} M_2^{\text{DM}} = & \frac{2}{3}S(S+1)\{(2\alpha_b^2 + 4\alpha_{ab}^2)[1 + \sin^2 \theta \cos^2 \varphi] \\ & + 4\beta_{ab}^2[1 + \sin^2 \theta \sin^2 \varphi] \\ & + (2\gamma_b^2 + 4\gamma_{ab}^2)[1 + \cos^2 \theta]\} \end{aligned} \quad (14)$$

For the crystal field, the expression for the second moment is given in terms of  $\tilde{D}_{\alpha\beta}$  by

$$\begin{aligned} M_2^{\text{CF}} = & \frac{4S(S+1)-3}{20 \cdot 4} \sum_j \{f_1[2\tilde{D}_{zz}^{(j)} - \tilde{D}_{xx}^{(j)} - \tilde{D}_{yy}^{(j)}]^2 \\ & + 10f_2(\tilde{D}_{xz}^{(j)} + \tilde{D}_{yz}^{(j)}) \\ & + f_3[(\tilde{D}_{xx}^{(j)} - \tilde{D}_{yy}^{(j)})^2 + 4\tilde{D}_{xy}^{(j)}]\} \end{aligned} \quad (15)$$

and again the sum over  $j$  is running over the four inequivalent Mn positions in the unit cell. The prefactors  $f_k$  allow to separate secular ( $f_1$ ) and non secular ( $f_2$  and  $f_3$ ) contributions. Again, the angular dependence is obtained by transforming the CF components into the crystallographic system and using the values listed in table I. The full expressions divided in secular and nonsecular parts are given in Appendix 2. It is important to point out here that both secular and nonsecular parts contain strong contributions proportional to  $\cos 4\varphi$  and  $\sin 4\theta$ , which should result in a  $\pi/2$  periodic modulation of the angular dependence. However, in

the sum  $M_2^{\text{CF}}(\text{secular}) + M_2^{\text{CF}}(\text{nonsecular})$  these contributions cancel each other for the case  $f_1 = f_2 = f_3$ . As the experimental data do not exhibit any  $\pi/2$  periodic modulation, only the latter case yields the appropriate description of the observed angular dependence. Under these circumstances the crystal field contribution reads e.g. for the  $ab$  plane

$$\begin{aligned} M_2^{\text{CF}}(ab) = & \frac{1}{80}[4S(S+1)-3]\{\frac{1}{2} \sum_j [2\tilde{D}_{zz}^{(j)} - \tilde{D}_{xx}^{(j)} - \tilde{D}_{yy}^{(j)}]^2 \\ & + \frac{5}{2} \sum_j [(\tilde{D}_{xx}^{(j)} - \tilde{D}_{yy}^{(j)})^2 + 4(\tilde{D}_{xy}^{(j)})^2] \\ & + 7 \sum_j [(\tilde{D}_{zy}^{(j)})^2 + (\tilde{D}_{xz}^{(j)})^2] \\ & + \sum_j [3(\tilde{D}_{zy}^{(j)})^2 - 3(\tilde{D}_{xz}^{(j)})^2 \\ & - (2\tilde{D}_{zz}^{(j)} - \tilde{D}_{xx}^{(j)} - \tilde{D}_{yy}^{(j)})(\tilde{D}_{xx}^{(j)} - \tilde{D}_{yy}^{(j)})] \cos 2\varphi\} \end{aligned} \quad (16)$$

The respective expressions for  $ac$  and  $bc$  plane are obtained by permutation of  $(x, y, z)$  and exchange of  $\varphi \rightarrow \theta$ , as indicated in Appendix 2.

## ANALYSIS AND DISCUSSION

As it is shown in Fig. 5, the linewidth data at 300 K are well described by the superposition of CF and DM contribution to the second moment (Eq. 12).

The superexchange integral  $J$  was estimated in mean-field approximation from the Curie-Weiss temperature  $\Theta_{\text{CW}} = C(4J_{ac} + 2J_b)$  with ferromagnetic in-plane coupling  $J_{ac}$  to four neighboring Mn ions and antiferromagnetic inter-plane coupling  $J_b$  to two neighboring Mn ions and the Curie constant  $C = S(S+1)/3k_{\text{B}}$  ( $k_{\text{B}}$ : Boltzmann constant). Assuming  $-J_{ac} = J_b = J$  and inserting the Mn<sup>3+</sup> spin  $S = 2$  and  $\Theta_{\text{CW}} = 111$  K [17], we obtain  $J = 14$  K. Both DM and CF interaction are of equal order of magnitude about 1 K. The DM interaction  $d_1 = 1.00(5)$  K along the antiferromagnetically coupled  $b$  axis is about three times larger than  $d_2 = 0.30(3)$  K within the ferromagnetically coupled  $ac$  plane. The absolute values of the crystal field parameters  $D = 0.73(2)$  K and  $E = -0.63(2)$  K are of nearly equal strength indicating comparable axial ( $D$ ) and rhombic ( $E$ ) distortions of the MnO<sub>6</sub> octahedra.

The angular dependence of the resonance linewidth at 200 K is well fitted with similar but slightly smaller parameters ( $d_1 = 1.00(5)$  K,  $d_1 = 0.26(3)$  K,  $D = 0.61(3)$  K,  $E = -0.58(3)$  K) in Fig. 6. In addition, the resonance field ( $g = 1.965$ ) can be described by similar crystal field parameters as the linewidth, thereby showing good agreement of static and dynamic susceptibility. As the

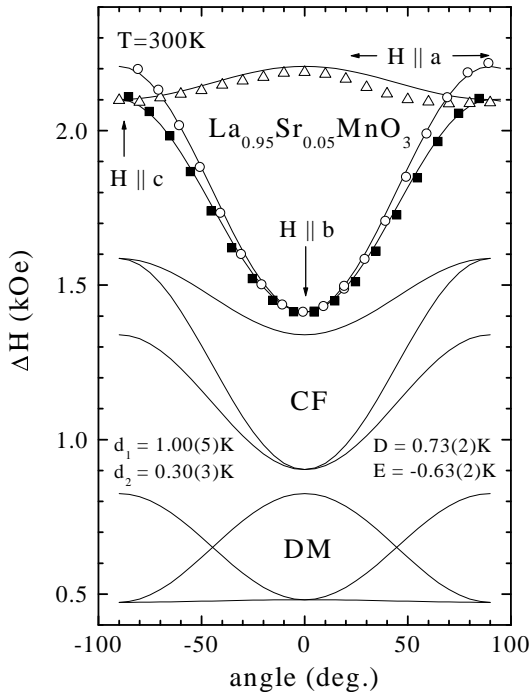


FIG. 5: Angular dependence of the ESR linewidth  $\Delta H$  in  $\text{La}_{0.95}\text{Sr}_{0.05}\text{MnO}_3$  for the magnetic field applied within the three crystallographic planes at 300 K. The solid lines represent the fit with equation 12. The lines below illustrate the contributions of CF and DM interaction, respectively

derivation of the linewidth was carried out in the high-temperature limit ( $T \gg \Theta_{\text{CW}}$ ), where it approximates an asymptotic value  $\Delta H(\infty)$ , we have to take into account, that the fit parameters  $D$ ,  $E$ ,  $d_1$  and  $d_2$  should reflect the temperature dependence. According to Huber *et al.* [11] far apart from any magnetic or structural transitions, the temperature dependence can be approximated by the quotient of the single-ion Curie susceptibility and the experimental Curie-Weiss susceptibility as

$$\Delta H(T) = \frac{T - \Theta_{\text{CW}}}{T} \Delta H(\infty). \quad (17)$$

Taking into account that the square of CF and DM parameters appears in the formulae for the second moment, we can extrapolate these parameters to  $T \rightarrow \infty$  via the square root of Eq. 17. Using the data at 300 K, which is far above magnetic order, we have to multiply the parameters by a factor 1.26 and get  $D(\infty) = 0.91$  K,  $E(\infty) = -0.79$  K,  $d_1(\infty) = 1.26$  K and  $d_2(\infty) = 0.38$  K. Comparing the values at 200 K, one expects a reduction of the parameters by approximately 15% with respect to

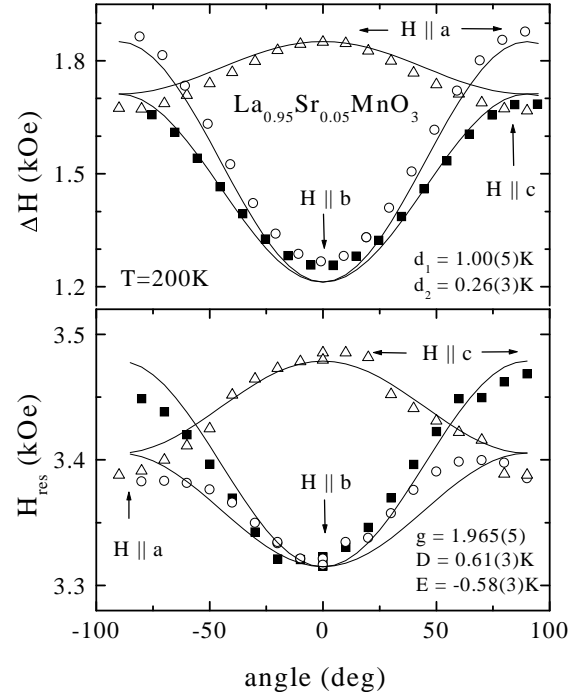


FIG. 6: Angular dependence of the ESR linewidth  $\Delta H$  (upper frame) and corrected resonance field  $H_{\text{res}}$  (lower frame) in  $\text{La}_{0.95}\text{Sr}_{0.05}\text{MnO}_3$  for the magnetic field applied within the three crystallographic planes at 200 K. The solid lines represent the fit with equations 12 and 11, respectively.

300 K. Indeed, this is well fulfilled, despite the onset of the critical behavior on approaching magnetic order at 140 K, only  $d_1$  remains unchanged.

The equations for the resonance field already contain the temperature dependence within the magnetization  $M(T)$ . For this reason it should be better described by the high-temperature values of the CF parameters than by the temperature dependent ones, which is the case at 200 K. Due to the rather large uncertainty in the determination of the resonance field and the proximity of the critical temperature region, this discrepancy is not assumed to be of significant importance. Thus, at 300 K the amplitude of the uncorrected resonance-field anisotropy is nicely reproduced by the high-temperature values of the CF parameters as  $H_{\text{res}}^{\text{max}} - H_{\text{res}}^{\text{min}} = 95$  Oe.

The strength of CF and DM interaction was independently determined from orientation dependent magnetization data [26], measured at 4.2 K in a  $\text{La}_{0.95}\text{Sr}_{0.05}\text{MnO}_3$  single crystal of the same batch as used in our ESR experiments. In combination with antiferromagnetic resonance measurements it was shown there,

that the ground state ( $T < T_N$ ) exhibits a canted antiferromagnetic structure, which rules out any phase separation in ferromagnetic and antiferromagnetic regions. Within the two-sublattice model Pimenov *et al.* obtained (after translation to our Hamiltonian in units of Kelvin) to the following parameters from the magnetization data [26]:  $J = 13.2$  K,  $K_z = -2E = 0.93$  K,  $K_x = D - E = 0.95$  K, and  $G = \sin(155^\circ)d_1 = 1.18$  K. These results are in good agreement with our findings, as the values of the CF parameters  $D = 0.48$  K and  $E = -0.47$  K are essentially equal. The DM contribution is of similar strength, where  $d_2$  was neglected. Thus, we could confirm the validity of their model from a microscopic point of view.

ESR studies by Huber *et al.* in  $\text{LaMnO}_3$  [11] and Tovar *et al.* [12] in the series  $\text{LaMnO}_{3+\delta}$  revealed values comparable to our parameters. For pure  $\text{LaMnO}_3$ , they use the CF parameter  $D = 1.92$  K determined by Moussa *et al.* from neutron-scattering experiments [27] and estimate the DM contribution as  $d \approx 0.8$  K. For an oxygen excess  $\delta = 0.03$  with a transition temperature  $T_{\text{JT}} = 600$  K comparable to  $\text{La}_{0.95}\text{Sr}_{0.05}\text{MnO}_3$ , the CF parameter  $D$  is found to be about 20% smaller than in the pure compound, whereas the DM interaction remains essentially unchanged at  $d \approx 0.8$  K. Though these data were measured in polycrystalline samples, where no distinction between axial( $D$ ) and rhombic( $E$ ) CF parameters and the inter-plane and intra-plane DM interaction could be made, their results agree with ours within a factor of 2.

The fact, that the two CF parameter are of comparable strength is of particular importance for the picture of orbital order in  $\text{LaMnO}_3$ . Many illustrations of the orbitally ordered state invoke the ordering of  $d_{3z^2-r^2}$  orbitals (e.g. [6, 8, 28]), as originally supposed by Goodenough [5] in order to describe the antiferromagnetic superexchange. So far this picture has been widely applied and in the absence of an experimentum crucis, which directly probes not only the electron-electron interaction induced by orbital order (which resonant X-Ray scattering is assumed to be able to [6]) but also reveals the kind of orbitals involved (which could not be identified by X-Ray resonant scattering [29]), it is the obvious choice in view of the observed axial distortion of the  $\text{MnO}_6$  octahedra.

Considering the equal contributions of  $D$  and  $E$ , we conclude that this picture of an ordering of  $d_{3z^2-r^2}$  orbitals has to be modified as it results in  $E = 0$  in contradiction to our findings, which are also in agreement with the results of Pimenov *et al.* [26]. In a local coordinate system the orbital of the  $e_g$  electron is a superposition  $\psi_{g,e} = c_1\phi_{3z^2-r^2} \pm c_2\phi_{x^2-y^2}$  [30], where  $c_1 = 0.8$  and  $c_2 = 0.6$  denote the orbital mixing coefficients down to lowest temperatures as reported by Rodriguez-Carvajal *et al.* [7] on the base of neutron-diffraction studies. Matsumoto [30] found in second order perturbation theory the following formula for the CF parameter  $E$

$$E = -2\sqrt{3}\frac{\lambda^2}{\Delta}c_1c_2, \quad (18)$$

with the spin-orbit coupling  $\lambda$  and the energy separation  $\Delta$  between the  $^5E_g$  ground state and  $^3T_{1g}$ . This formula qualitatively confirms our conclusions, as not only the sign of our parameters is reproduced but also both orbital mixing coefficients must not be negligibly small in order to explain the observed rhombic CF parameter  $E$ .

## CONCLUSION

We performed a systematic investigation of the angular dependence of the paramagnetic resonance in the Jahn-Teller distorted orthorhombic phase in  $\text{La}_{0.95}\text{Sr}_{0.05}\text{MnO}_3$  single crystals. We presented a comprehensive analysis for the resonance linewidth in high-temperature approximation, which takes into account the microscopic geometry of the four inequivalent Mn positions in the orthorhombic unit cell based on the structural data determined for  $\text{LaMnO}_3$  by Huang *et al.* [13]. The crystal-field parameters for all Mn positions and the Dzyaloshinsky-Moriya interaction for nearest-neighbor Mn ions along the  $b$  axis as well as in the  $ac$  plane were successfully extracted as  $D(\infty) = 0.91$  K,  $E(\infty) = -0.79$  K,  $d_1(\infty) = 1.26$  K and  $d_2(\infty) = 0.38$  K. These findings shed new light on the microscopic picture of orbital ordering and spin-spin interaction in these compounds.

## ACKNOWLEDGEMENTS

It is a pleasure to thank K.-H. Höck for fruitful discussions. This work was supported in part by the BMBF under contract no. 13N6917 (EKM), by the Deutsche Forschungsgemeinschaft (DFG) via the Sonderforschungsbereich 484 and DFG-project No. 436-RUS 113/566/0, and by INTAS (project no. 97-30850). The work of M. V. Eremin was partially supported by RFBR grant no. 00-02-17597 and NIOKR Tatarstan.

## APPENDIX 1: Relative superexchange strength and sign of parameters

We consider the Hamiltonian of superexchange coupling between two  $\text{Mn}^{3+}$  ions on lattice sites ( $A$ ) and ( $B$ )

$$\mathcal{H} = J_{AB}(\mathbf{S}_A \cdot \mathbf{S}_B) = 2 \sum_{\eta, \zeta} j_{\eta\zeta, \zeta\eta} (\mathbf{s}_\eta \cdot \mathbf{s}_\zeta) \quad (19)$$

where  $j_{\eta\zeta',\zeta\eta'}$  denote the superexchange parameters via one electron states, the symbol  $\eta$  refers to the Mn( $A$ ) state whereas  $\zeta$  refers to Mn( $B$ ). In the ground state Mn $^{3+}$  ions have maximum spin. Therefore we can write:

$$J_{AB} = \frac{1}{2S_A S_B} \sum_{\eta,\zeta} j_{\eta\zeta,\zeta\eta} \quad (20)$$

Along the  $b$  axis, the superexchange is mainly realized via the  $|y^2 - x^2\rangle - |y^2 - z^2\rangle$  channel and has antiferromagnetic character. Within the  $ac$  plane the ferromagnetic coupling is mainly transferred via the channel  $|y^2 - x^2\rangle - |y^2 - z^2\rangle$ . The relevant states like  $|y^2 - x^2\rangle$  and  $|y^2 - z^2\rangle$  are mutually orthogonal and yield negative  $j_{y^2-x^2,y^2-z^2}$ .

The Dzyaloshinsky-Moriya parameter  $d_{AB}$  from equation 7 can be derived from the following expression

$$G_{AB}^\perp = -\frac{i}{2S_A S_B} \left\{ \sum_{\eta,\zeta,\zeta'} \frac{\xi_A}{|\Delta_{\eta,\eta'}|} j_{\eta\zeta,\zeta\eta'} \langle \eta' | l_A^{(\perp)} | \eta \rangle - \sum_{\eta,\zeta,\eta'} \frac{\xi_B}{|\Delta_{\zeta,\zeta'}|} j_{\eta\zeta',\zeta\eta} \langle \zeta' | l_B^{(\perp)} | \zeta \rangle \right\} \quad (21)$$

here  $i$  is the imaginary unit,  $\xi_A$  and  $\xi_B$  are spin-orbit coupling constants,  $\Delta_{\zeta,\zeta'}$  denotes the energy splitting between the states  $\zeta$  and  $\zeta'$ .  $l_A^{(\perp)}$  and  $l_B^{(\perp)}$  are components of the one-electron orbital momentum perpendicular to the plane, built up by Mn( $A$ )-bridging oxygen(O) -Mn( $B$ ),  $\mathbf{n}_{AO}$  and  $\mathbf{n}_{BO}$  are the corresponding unit vectors along the Mn-O bonds.  $j_{\eta\zeta',\zeta\eta}$  and  $j_{\eta\zeta,\zeta\eta'}$  can be expressed via a product of dimensionless transfer integrals  $\lambda_\sigma, \lambda_\pi, \lambda_s$  corresponding to Mn-O bonds [31, 32]

In order to explain the main features for the moment, we shall simplify the orbital ordering as  $|y^2 - z^2\rangle$  like states along the  $b$  axis and alternating ordering like  $|y^2 - z^2\rangle, |y^2 - x^2\rangle$  within the  $(ac)$  plane. Then one has the following situation:

1) Along the  $b$  axis, the largest contribution to the superexchange comes from  $j_{y^2-z^2,y^2-z^2,y^2-z^2,y^2-z^2}$ , yielding

$$J_b \sim \frac{1}{8} \left( \frac{3}{4} \right)^2 [\lambda_\sigma^2 \cos \vartheta + \lambda_s^2]^2 \quad (22)$$

and for the DM vector the most important term is  $j_{y^2-z^2,y^2-z^2,y^2-z^2,yz}$ , which leads to

$$d_1 \sim -\frac{\xi}{2\Delta} \left( \frac{3}{4} \right)^{3/2} [\lambda_\sigma^2 \cos \vartheta + \lambda_s^2] \lambda_\pi \lambda_\sigma \quad (23)$$

2) Within the  $ac$  plane, the major contribution to the superexchange comes from  $j_{y^2-z^2,y^2-x^2,y^2-x^2,y^2-z^2}$  and hence

$$J_{ac} \sim -\frac{J_H}{8U} \left( \frac{3}{4} \right) [\lambda_\sigma^2 \cos \vartheta + \lambda_s^2]^2 \quad (24)$$

whereas for  $DM$  vector the most important term is  $j_{y^2-z^2,y^2-z^2,y^2-z^2,xy}$  and therefore

$$d_2 \sim \frac{J_H}{4U \Delta} \left( \frac{\xi}{4} \right)^{1/2} [\lambda_\sigma^2 \cos \vartheta + \lambda_s^2] \lambda_\pi \lambda_\sigma \quad (25)$$

here  $\vartheta$  is the angle between  $\mathbf{n}_{AO}$  and  $\mathbf{n}_{OB}$  vectors,  $J_H$  denotes the intra-atomic Hund's exchange parameter,  $U$  is the charge-transfer energy between the Mn ions. From these expression one can clearly see that the relative sign of parameters  $d_{AB}$  along the  $b$  axis ( $d_1$  in text) and  $d_{AB}$  within  $(ac)$  plane ( $d_2$  in text) are different as well as superexchange parameters  $J_b$  and  $J_{ac}$ .

## APPENDIX 2: remarks on the calculation

Here we outline the transformation between the crystallographic system  $(x, y, z) \parallel (a, b, c)$  and the coordinate system  $(\tilde{x}, \tilde{y}, \tilde{z})$  with the  $\tilde{z}$ -axis parallel to the applied magnetic field  $H$  and rotated by the polar angle  $\theta$  and the azimuth angle  $\varphi$  with respect to the crystallographic system. Assuming an isotropic  $g$  value, the DM vector transforms like the space coordinates:

$$\begin{aligned} \tilde{G}_{ij}^x &= G_{ij}^x \cos \theta \cos \varphi + G_{ij}^y \cos \theta \sin \varphi - G_{ij}^z \sin \theta \\ \tilde{G}_{ij}^y &= G_{ij}^y \cos \varphi - G_{ij}^x \sin \varphi \\ \tilde{G}_{ij}^z &= G_{ij}^x \sin \theta \cos \varphi + G_{ij}^y \sin \theta \sin \varphi + G_{ij}^z \cos \theta \end{aligned} \quad (26)$$

The crystal-field components  $D_{\alpha\beta} \propto (\alpha\beta)/R^2$  transform like the product of the oxygen coordinates  $\alpha$  and  $\beta$ .

For the angular dependence of the resonance field we need the following relations:

$$1) ab \text{ plane } (\theta = \frac{\pi}{2})$$

$$\begin{aligned} \sum_j (\tilde{D}_{xx}^{(j)} + \tilde{D}_{yy}^{(j)} - 2\tilde{D}_{zz}^{(j)}) &= \frac{1}{2} \sum_i (2D_{zz}^{(i)} - D_{xx}^{(i)} - D_{yy}^{(i)}) \\ &\quad - \frac{3}{2} \sum_i (D_{xx}^{(i)} - D_{yy}^{(i)}) \cos 2\varphi \\ \sum_j (\tilde{D}_{xx}^{(j)} - \tilde{D}_{yy}^{(j)} \pm 2i\tilde{D}_{xy}^{(j)}) &= \frac{1}{2} \sum_i (2D_{zz}^{(i)} - D_{xx}^{(i)} - D_{yy}^{(i)}) \\ &\quad + \frac{1}{2} \sum_i (D_{xx}^{(i)} - D_{yy}^{(i)}) \cos 2\varphi \end{aligned}$$

$$2) ac \text{ plane } (\varphi = 0)$$

$$\begin{aligned}\sum_j (\tilde{D}_{xx}^{(j)} + \tilde{D}_{yy}^{(j)} - 2\tilde{D}_{zz}^{(j)}) &= \frac{1}{2} \sum_i (2D_{yy}^{(i)} - D_{zz}^{(i)} - D_{xx}^{(i)}) \\ &\quad - \frac{3}{2} \sum_i (D_{zz}^{(i)} - D_{xx}^{(i)}) \cos 2\theta\end{aligned}$$

$$\begin{aligned}\sum_j (\tilde{D}_{xx}^{(j)} - \tilde{D}_{yy}^{(j)} \pm 2i\tilde{D}_{xy}^{(j)}) &= -\frac{1}{2} \sum_i (2D_{yy}^{(i)} - D_{zz}^{(i)} - D_{xx}^{(i)}) \\ &\quad - \frac{1}{2} \sum_i (D_{zz}^{(i)} - D_{xx}^{(i)}) \cos 2\theta\end{aligned}$$

3) bc plane ( $\varphi = \frac{\pi}{2}$ )

$$\begin{aligned}\sum_j (\tilde{D}_{xx}^{(j)} + \tilde{D}_{yy}^{(j)} - 2\tilde{D}_{zz}^{(j)}) &= \frac{1}{2} \sum_i (2D_{xx}^{(i)} - D_{yy}^{(i)} - D_{zz}^{(i)}) \\ &\quad - \frac{3}{2} \sum_i (D_{zz}^{(i)} - D_{yy}^{(i)}) \cos 2\theta\end{aligned}$$

$$\begin{aligned}\sum_j (\tilde{D}_{xx}^{(j)} - \tilde{D}_{yy}^{(j)} \pm 2i\tilde{D}_{xy}^{(j)}) &= -\frac{1}{2} \sum_i (2D_{xx}^{(i)} - D_{yy}^{(i)} - D_{zz}^{(i)}) \\ &\quad - \frac{1}{2} \sum_i (D_{zz}^{(i)} - D_{yy}^{(i)}) \cos 2\theta\end{aligned}$$

Concerning the linewidth, the second moment due to DM interaction can be expressed in crystallographic coordinates as

$$\begin{aligned}M_2^{\text{DM}} &= \frac{2}{3}S(S+1)\{\sum_{i,j}(G_{ij}^x)^2[1 + \sin^2\theta \cos^2\varphi] \\ &\quad + \sum_{i,j}(G_{ij}^y)^2[1 + \sin^2\theta \sin^2\varphi] \\ &\quad + \sum_{i,j}(G_{ij}^z)^2[1 + \cos^2\theta] + \sum_{i,j}G_{ij}^x G_{ij}^y \sin 2\varphi \sin^2\theta \\ &\quad + \sum_{i,j}G_{ij}^x G_{ij}^z \sin 2\theta \cos\varphi + \sum_{i,j}G_{ij}^y G_{ij}^z \sin 2\theta \sin\varphi\}\end{aligned}\quad (27)$$

On evaluation of  $M_2^{\text{DM}}$ , it turns out that all sums over cross terms  $G_{ij}^\alpha G_{ij}^\beta$  with  $\alpha \neq \beta$  vanish and the remaining sums over  $i$ , which are equal for all Mn sites  $j$ , read:

$$\begin{aligned}\sum_i (G_{ij}^x)^2 &= 2\alpha_b^2 + 4\alpha_{ab}^2 \\ \sum_i (G_{ij}^y)^2 &= 4\beta_{ab}^2 \\ \sum_i (G_{ij}^z)^2 &= 2\gamma_b^2 + 4\gamma_{ab}^2\end{aligned}\quad (28)$$

Concerning the contribution of the crystal field  $M_2^{\text{CF}}$ , it is clear from values listed in Table I that many sums over four Mn position vanish in the crystallographic system, which is very convenient. For example

$$\begin{aligned}\sum_j (D_{zz}^{(j)} - D_{yy}^{(j)})D_{yz}^{(j)} &= \sum_j (D_{zz}^{(j)} - D_{xx}^{(j)})D_{xz}^{(j)} \\ &= \sum_j (D_{xx}^{(j)} - D_{yy}^{(j)})D_{xy}^{(j)} \\ &= \sum_j [2D_{xx}^{(j)} - D_{zz}^{(j)} - D_{yy}^{(j)}]D_{yz}^{(j)} \\ &= \sum_j [2D_{yy}^{(j)} - D_{xx}^{(j)} - D_{zz}^{(j)}]D_{xz}^{(j)} \\ &= \sum_j [2D_{zz}^{(j)} - D_{xx}^{(j)} - D_{yy}^{(j)}]D_{xy}^{(j)} = 0\end{aligned}$$

From symmetry point of view it is understandable, because there are mirror planes within  $ab$ ,  $ac$  and  $bc$  planes. Having in mind these properties, after some manipulation we arrive to the following formulae for the secular part of  $M_2^{\text{CF}}$  (i.e. when factors  $f_2$  and  $f_3$  are equal to zero) and nonsecular parts (we consider the case  $f_2 = f_3$ ):

1)  $ab$  plane ( $\theta = \frac{\pi}{2}$ ):

$$\begin{aligned}M_2^{\text{CF}}(\text{sec}) &= \frac{1}{80}[4S(S+1) - 3]\{\frac{1}{4}\sum_j [2D_{zz}^{(j)} - D_{xx}^{(j)} - D_{yy}^{(j)}]^2 \\ &\quad + \frac{9}{8}\sum_j [(D_{xx}^{(j)} - D_{yy}^{(j)})^2 + 4(D_{xy}^{(j)})^2] \\ &\quad - \frac{3}{2}\sum_j [2D_{zz}^{(j)} - D_{xx}^{(j)} - D_{yy}^{(j)}](D_{xx}^{(j)} - D_{yy}^{(j)}) \cos 2\varphi \\ &\quad + \frac{9}{8}\sum_j [(D_{xx}^{(j)} - D_{yy}^{(j)})^2 - 4(D_{xy}^{(j)})^2] \cos 4\varphi\}\end{aligned}\quad (29)$$

$$\begin{aligned}M_2^{\text{CF}}(\text{non}) &= \frac{1}{80}[4S(S+1) - 3]\{\frac{1}{4}\sum_j [2D_{zz}^{(j)} - D_{yy}^{(j)} - D_{xx}^{(j)}]^2 \\ &\quad + \frac{11}{8}\sum_j [(D_{yy}^{(j)} - D_{xx}^{(j)})^2 + 4(D_{xy}^{(j)})^2] \\ &\quad + 7\sum_j [(D_{zy}^{(j)})^2 + (D_{xz}^{(j)})^2] \\ &\quad + \sum_j \{\frac{1}{2}[2D_{zz}^{(j)} - D_{yy}^{(j)} - D_{xx}^{(j)}](D_{xx}^{(j)} - D_{yy}^{(j)}) \\ &\quad + 3[(D_{zy}^{(j)})^2 - (D_{xz}^{(j)})^2]\} \cos 2\varphi \\ &\quad - \frac{9}{8}\sum_j [(D_{xx}^{(j)} - D_{yy}^{(j)})^2 - 4(D_{xy}^{(j)})^2] \cos 4\varphi\}\end{aligned}\quad (30)$$

2)  $ac$  plane ( $\varphi = 0$ ): like  $ab$  plane with permutation  $x, y, z \rightarrow z, x, y$  and exchange  $\varphi \rightarrow \theta$ .

3)  $bc$  plane ( $\varphi = \frac{\pi}{2}$ ): like  $ab$  plane with permutation  $x, y, z \rightarrow z, y, x$  and exchange  $\varphi \rightarrow \theta$ .

---

[1] A. K. Bogush, V. I. Pavlov, and L. V. Balyko, *Cryst. Res. Technol.* **18**, 589 (1983); M. Paraskevopoulos, F. Mayr, C. Hartinger, A. Pimenov, J. Hemberger, P. Lunkenheimer, A. Loidl, A. A. Mukhin, V. Yu. Ivanov, and A. M. Balbashov, *J. Magn. Magn. Mat.* **211**, 118 (2000); A. Urushibara, Y. Moritomo, T. Arima, A. Asamitsu, G. Kido, and Y. Tokura, *Phys. Rev. B* **51**, 14103 (1995); J.-S. Zhou, J. B. Goodenough, A. Asamitsu, and Y. Tokura, *Phys. Rev. Lett.* **79**, 3234 (1997).

[2] D. Khomskii, cond-mat/0104517.

[3] J. P. Hill, C. S. Nelson, M. v. Zimmermann, V.-J. Kim, Doon Gibbs, D. Casa, B. Keimer, Y. Murakami, C. Venkataraman, T. Gog, Y. Tomioka, Y. Tokura, V. Kiryukhi, T.Y. Koo, and S.-W. Cheong, cond-mat/01050643.

[4] E. Dagotto, T. Hotta, and A. Moreo, *Phys. Rep.* **344**, 1 (2001).

[5] J. B. Goodenough, A. Wold, R. J. Arnott, and N. Menyuk, *Phys. Rev.* **124**, 373 (1961).

[6] Y. Murakami, J. P. Hill, D. Gibbs, M. Blume, I. Koyama, M. Tanaka, H. Kawata, T. Arima, Y. Tokura, K. Hirota, and Y. Endoh, *Phys. Rev. Lett.* **81**, 582 (1998).

[7] J. Rodriguez-Carvajal, M. Hennion, F. Moussa, A. H. Moudden, L. Pinsard, and A. Revcolevschi, *Phys. Rev. B* **57**, R3189 (1998).

[8] E. Saitoh, S. Okamoto, K. T. Takahashi, K. Tobe, K. Yamamoto, T. Kimura, S. Ishihara, S. Maekawa, and Y. Tokura, *Nature* **410**, 180 (2001).

[9] E. Granado, N. O. Moreno, A. Garcia, J. A. Sanjurjo, C. Rettori, I. Torriani, S. B. Oseroff, J. J. Neumeier, K. J. McClellan, S.-W. Cheong, and Y. Tokura, *Phys. Rev. B* **58**, 11435 (1998).

[10] V. A. Ivanshin, J. Deisenhofer, H.-A. Krug von Nidda, A. Loidl, A. A. Mukhin, A. M. Balbashov and M. V. Eremin, *Phys. Rev. B* **61**, 6213 (2000).

[11] D. L. Huber, G. Alejandro, A. Caneiro, M.T. Causa, F. Prado, M. Tovar, and S. B. Oseroff, *Phys. Rev. B* **60**, 12155 (1999).

[12] M. Tovar, G. Alejandro, A. Butera, A. Caneiro, M.T. Causa, F. Prado, and R. D. Sánchez, *Phys. Rev. B* **60**, 10199 (1999).

[13] Q. Huang, A. Santoro, J. W. Lynn, R. W. Erwin, J. A. Borchers, J. L. Peng, and R. L. Greene, *Phys. Rev. B* **55**, 14987 (1997).

[14] S. E. Barnes, *Adv. Phys.* **30**, 801 (1981).

[15] H. Benner, M. Brodehl, H. Seitz, and J. Wiese, *J. Phys. C* **16** 6011 (1983).

[16] A. A. Mukhin, V. Yu. Ivanov, V. D. Travkin, S. P. Lebedev, A. Pimenov, A. Loidl, and A. M. Balbashov, *JETP Letters*, **68**, No.4, 356 (1998).

[17] M. Paraskevopoulos, F. Mayr, J. Hemberger, A. Loidl, R. Heichele, D. Maurer, V. Müller, A. M. Mukhin, A. M. Balbashov, *J. Phys.: Condens. Matter* **12**, 3993 (2000).

[18] A. Abragam and B. Bleaney, *EPR of Transition Ions*, Clarendon Press, Oxford 1970.

[19] T. Moriya, *Phys. Rev. Lett.* **4**, 228 (1960); *Phys. Rev.* **120**, 91 (1960).

[20] F. Keffer, *Phys. Rev.* **126**, 896 (1962).

[21] A. S. Moskvin and I. G. Bostrem, *Sov. Phys. Solid State*, **19**, 1532 (1977).

[22] N. O. Moreno, P. G. Pagliuso, C. Rettori, J. S. Gardner, J. L. Sarrao, and J. D. Thompson, D. L. Huber, J. F. Mitchell, J. J. Martinez, and S. B. Oseroff, *Phys. Rev. B* **63**, 174413 (2001).

[23] P. W. Anderson and P. R. Weiss, *Rev. Mod. Phys.* **25**, 269 (1953).

[24] T. G. Castner, Jr. and M. S. Seehra, *Phys. Rev. B* **4**, 38 (1971).

[25] Z. G. Soos, K. T. McGregor, T. T. P. Cheung, and A. J. Silverstein, *Phys. Rev. B* **16**, 3036 (1977).

[26] A. Pimenov, M. Biberacher, D. Ivannikov, A. Loidl, V. Yu. Ivanov, A. A. Mukhin, and A. M. Balbashov, *Phys. Rev. B* **62**, 5685 (2000).

[27] F. Moussa, M. Hennion, J. Rodriguez-Carvajal, A. H. Moudden, L. Pinsard, and A. Revcolevschi, *Phys. Rev. B* **54**, 15149 (1996).

[28] Igor Solov'yev, Noriaki Hamada, and Kiyoyuki Terakura, *Phys. Rev. Lett.* **76**, 4825 (1996).

[29] S. Ishihara and S. Maekawa, *Phys. Rev. B* **58**, 13442 (1998).

[30] G. Matsumoto, *J. Phys. Soc. Jpn.* **29**, 606 (1970).

[31] P. W. Anderson, *Phys. Rev.* **115**, 2 (1959).

[32] M.V. Eremin, *Opt. Spectrosc.* **68**, 502 (1990).

TABLE I: Crystal field parameters for different Mn positions in the unit cell.

$D_{\alpha\beta}$ \ Mn (j)- site	$(0, 0, \frac{1}{2})$	$(\frac{1}{2}, 0, 1)$	$(0, \frac{1}{2}, \frac{1}{2})$	$(\frac{1}{2}, \frac{1}{2}, 1)$
$D_{xx}^{(j)}$	$D_{xx}^{(1)}$	$D_{xx}^{(1)}$	$D_{xx}^{(1)}$	$D_{xx}^{(1)}$
$D_{yy}^{(j)}$	$D_{yy}^{(1)}$	$D_{yy}^{(1)}$	$D_{yy}^{(1)}$	$D_{yy}^{(1)}$
$D_{zz}^{(j)}$	$D_{zz}^{(1)}$	$D_{zz}^{(1)}$	$D_{zz}^{(1)}$	$D_{zz}^{(1)}$
$D_{xy}^{(j)}$	$D_{xy}^{(1)}$	$D_{xy}^{(1)}$	$-D_{xy}^{(1)}$	$-D_{xy}^{(1)}$
$D_{xz}^{(j)}$	$D_{xz}^{(1)}$	$-D_{xz}^{(1)}$	$D_{xz}^{(1)}$	$-D_{xz}^{(1)}$
$D_{yz}^{(j)}$	$D_{yz}^{(1)}$	$-D_{yz}^{(1)}$	$-D_{yz}^{(1)}$	$D_{yz}^{(1)}$

TABLE II: DM vector components for different pairs of Mn ions in the unit cell of  $\text{LaMnO}_3$ .

Mn(i)-site \ Mn (j)-site	$(0, 0, \frac{1}{2})$	$(\frac{1}{2}, 0, 1)$	$(0, \frac{1}{2}, \frac{1}{2})$	$(\frac{1}{2}, \frac{1}{2}, 1)$
$(x_j, y_j + \frac{1}{2}, z_j)$	$(-\alpha_b, 0, -\gamma_b)$	$(\alpha_b, 0, -\gamma_b)$	$(-\alpha_b, 0, -\gamma_b)$	$(\alpha_b, 0, -\gamma_b)$
$(x_j, y_j - \frac{1}{2}, z_j)$	$(\alpha_b, 0, \gamma_b)$	$(-\alpha_b, 0, \gamma_b)$	$(\alpha_b, 0, \gamma_b)$	$(-\alpha_b, 0, \gamma_b)$
$(x_j + \frac{1}{2}, y_j, z_j - \frac{1}{2})$	$(-\alpha_{ac}, \beta_{ac}, -\gamma_{ac})$	$(\alpha_{ac}, -\beta_{ac}, \gamma_{ac})$	$(\alpha_{ac}, \beta_{ac}, \gamma_{ac})$	$(-\alpha_{ac}, -\beta_{ac}, -\gamma_{ac})$
$(x_j - \frac{1}{2}, y_j, z_j - \frac{1}{2})$	$(-\alpha_{ac}, \beta_{ac}, \gamma_{ac})$	$(\alpha_{ac}, -\beta_{ac}, -\gamma_{ac})$	$(\alpha_{ac}, \beta_{ac}, -\gamma_{ac})$	$(-\alpha_{ac}, -\beta_{ac}, \gamma_{ac})$
$(x_j - \frac{1}{2}, y_j, z_j + \frac{1}{2})$	$(-\alpha_{ac}, \beta_{ac}, -\gamma_{ac})$	$(\alpha_{ac}, -\beta_{ac}, \gamma_{ac})$	$(\alpha_{ac}, \beta_{ac}, \gamma_{ac})$	$(-\alpha_{ac}, -\beta_{ac}, -\gamma_{ac})$
$(x_j + \frac{1}{2}, y_j, z_j + \frac{1}{2})$	$(-\alpha_{ac}, \beta_{ac}, \gamma_{ac})$	$(\alpha_{ac}, -\beta_{ac}, -\gamma_{ac})$	$(\alpha_{ac}, \beta_{ac}, -\gamma_{ac})$	$(-\alpha_{ac}, -\beta_{ac}, \gamma_{ac})$